Desalination and Water Treatment
www.deswater.com

doi: 10.5004/dwt.2020.25034

179 (2020) 160–171
March

Novel magnetized carbon core-shell impregnated with lanthanum as an adsorbent for uptake of fluoride from aquatic systems, studied by response surface methodology

Mansoureh Yaghini, Hossein Faghihian*

Department of Chemistry, Shahreza Branch, Islamic Azad University, Shahreza, Iran, Tel. +983137934624; email: faghihian@iaush.ac.ir (H. Faghihian), yaghini_m@yahoo.com (M. Yaghini)

Received 25 May 2019; Accepted 14 October 2019

ABSTRACT

The presence of excessive fluoride in drinking water causes serious human health and environmental problems. In this study, a novel sorbent was synthesized for efficient uptake of fluoride ions from aquatic systems. The sorbent was prepared by impregnation of magnetized carbon core-shell (Fe_3O_4@C) with lanthanum and was identified by Fourier transform infrared, Brunauer–Emmett–Teller, transmission electron microscopy, scanning electron microscopy, X-ray diffraction and energy dispersive X-ray analysis methods and its magnetic property was evaluated by vibrating sample magnetometer method. The adsorption experiments were designed via response surface methodology. The experimental parameters including pH, contacting time, initial fluoride concentration, and adsorbent dose were selected as independent variables and their influence on the adsorption of fluoride was studied. The method indicated that the second-order equation was the most adequate equation for optimizing the adsorption parameters. The variance of analysis also confirmed the fitness of the model. The maximal uptake of 20.75 mg g^{-1} was obtained. The selectivity of the synthesized sorbent was evaluated in the presence of co-existing species; chloride, nitrate, hydrogen carbonate, and hydroxyl anions. The results indicated that hydroxide and chloride ions had the most and the least interfering effects on the removal of fluoride respectively. The regeneration performance of the used adsorbent was evaluated. After three regeneration cycles, 73% of the initial capacity remained.

Keywords: Carbon magnetic core-shell; Response surface methodology; Fluoride elimination; Lanthanum

1. Introduction

Water is the most available solvent for many biological and chemical substances and hence is highly susceptible to contamination by many pollutants [1]. Many diseases are caused by inadequate treatment of contaminated drinking water [2]. Nowadays, increasing contamination of groundwater with fluoride is one of the main concerns across the world [3]. Fluoride is a persistent and non-biodegradable pollutant that can be concentrated in soil, plants, and human tissues [4]. The maximum permissible content of fluoride is 1.5 mg L^{-1} [5]. Therefore, the improvement of new methods for removal of the excess of fluoride to improve the access to safe drinking water is seriously needed [2,4].

A widespread range of technologies has been employed for reducing the fluoride content of water below permissible value, including chemical precipitation, membrane separation, electrocoagulation, flotation, oxidation, solvent extraction, evaporation, distillation, reverse osmosis, electrodialysis, ion exchange, and adsorption [5,6]. Among them, the adsorption method owing to cost-effectiveness, environmental friendliness, and ease of operation, is one of the

* Corresponding author.

most promising methods [5]. The preparation of an adequate adsorbent is the most determining factor for the successful defluorination process by the adsorption method. The sorption capacity, selectivity, chemical stability, regeneration ability, and the textural properties of the adsorbent are the most important factors that impress the adsorption process [7,8]. Various sorbents employed for the removal of fluoride include zeolites, porous and active carbons, metal oxides, hydroxides, biosorbent, iron and calcium-based adsorbents [9]. Carbon nanomaterials have been considered as potential adsorbents for water purification due to their good chemical stability, high surface area, structural diversity, and suitability for large-scale production [7]. Nano adsorbents have many advantages compared to their micro-sized counterparts, but the greatest practical limitation of nano-sized adsorbent is the difficulties associated with separation from the solutions [10]. However, magnetization of the adsorbent can be considered as an alternative way to eliminate this limitation. Magnetic separation compared to the conventional separation methods has several major advantages, such as high speed, effective control, accuracy and simplicity [11]. Therefore, in recent years, there has been enormous increases in the synthesis of magnetic composites based on Fe_3O_4 for application in adsorption and separation methods [12]. Although Fe_3O_4 particles have many advantages on magnetic separation, in practice they have two major limitations:

- Fe_3O_4 has low stability in strongly acidic media.
- Fe_3O_4 has limited surface functional groups [13].

These drawbacks can be controlled by changing the synthesis procedure to prepare core-shell composite in which the magnetic core is shielded by another resistive phase [14]. Many reports showed that magnetic materials shielded by carbon (Fe_3O_4@C) exhibited better performance over conventional Fe_3O_4/C composites [12]. However, the carbonaceous materials have a low affinity for inorganic pollutants, like fluoride, and show limited adsorption capacity. To overcome this difficulty, modification of activated carbons by various chemical species can be considered [15]. Fluoride ion is a highly electronegative ion with a small ionic radius and is classified as a hard base. It has strong reactivity toward multivalent cations such as aluminum(III)), iron(III), and lanthanum(III) [16]. Therefore, the impregnation of carbonaceous adsorbent by lanthanum can increase its adsorption capacity towards fluoride ions.

The adsorption experiments can be either performed by one factor at a time method or response surface methodology (RSM). The first method needs a large number of experiments, and cannot determine the interactions of the variables. Between the influencing variables cannot be evaluated. Therefore, to reduce the number of required experiments, to evaluate the interactions between experimental parameters, and to optimize the effect of influencing variables, the RSM is more reliable [17].

This research aimed to prepare a novel magnetized core-shell for efficient uptake of fluoride from aqueous solutions. The experimental variables including solution pH, contacting time, F^- concentration and dosage of adsorbent were evaluated by RSM techniques and central composite design.

2. Experiments

2.1. Chemicals and instruments

All chemicals including; NaF, HNO_3, CH_3COOH, NaOH, $NaNO_3$, $NaHCO_3$, NaCl, La $(NO_3)_3{\cdot}6H_2O$, $FeCl_3{\cdot}6H_2O$, $C_6H_{12}O_6{\cdot}H_2O$, CO $(NH_2)_2$, C_2H_5OH and $C_2H_6O_2CHO$ ethylene glycol (EG) were analytical grade and purchased from Merck Company (Germany). The morphology of the adsorbent was examined by transmission electron microscopy (TEM, S-100 KW208 Philips, Netherland). Fourier transforms infrared (FT-IR) spectra were prepared by the FTIR spectrophotometer (Perkin Elmer Spectrum 65, USA) by the use of KBr pellets. The powder X-ray patterns were taken by X'pert PRO, Philips, PW1730 diffractometer (Netherland). The scanning electron microscopy (SEM) images were taken by use of Zeiss Ultra 55 devise, MIRA3LMU, TESCAN Co., (Czech Republic) with an accelerating voltage of 15 kV. The energy dispersive X-ray analysis (EDX) analysis was performed by a MIRA3LMU spectrometer, TESCAN Co., (Czech Republic). The Brunauer–Emmett–Teller (BET) surface area was determined by the use of a BET Belsorp, Mini II instrument, BEL Company (Japan). The magnetic property of the adsorbents was evaluated by a vibrating sample magnetometer (VSM), MDKFT (Iran). A pH meter (Denver, Ultrabasic, UB-10, Germany) was used to measure the pH of the solutions. The concentration of fluoride was measured by a Sartorius PY-l01 F^- electrode (Germany).

2.2. Preparation of core-shell

The Fe_3O_4@C was synthesized through the solvothermal method described by Zheng et al. [18] by reacting to $FeCl_3{\cdot}6H_2O$, glucose, and $CO(NH_2)_2$ dissolved in EG. Briefly, a mixture containing 2.78 g of $FeCl_3{\cdot}6H_2O$, 5.56 g of urea, and 0.37 g of glucose dissolved in 111 mL of EG was prepared, was shaken for 45 min and then poured into a Teflon-lined autoclave. The autoclave was maintained at 200°C for 12 h. The product Fe_3O_4@C was separated and was rinsed respectively with distilled water and C_2H_5OH.

2.3. Impregnation of magnetic core-shell by lanthanum

Lanthanum was introduced into Fe_3O_4@C composite through the method described by Jose Rene Rangel-Mendez by using a lanthanum nitrate solution [15]. Briefly, 1.6 g of core-shell was added into 20 mL of lanthanum nitrate solution (0.3 M). The mixture was stirred for 10 h at 60°C. The supernatant solution was decanted and replaced with fresh La $(NO_3)_3$ solution. To ensure the maximal impregnation of lanthanum, the procedure was repeated three times. The solid (Fe_3O_4@C/La) was then removed by a magnet bar, washed thoroughly with distilled water and dried at 60°C for 6 h.

2.4. Optimizing of variables by RSM model

By conducting a series of batch experiments, the most influencing variables on the adsorption process were determined. Four variables including pH of the solution, contacting period, F^- content, and adsorbent dosage was selected. Levels of each variable were considered as +1, 0, and −1

for lowest, middle, and highest level, respectively [5]. The response of each variable, $Y(R)$ as a function of the selected variables were then measured as; pH (X_1), contacting time (X_2), F^- content (X_3), and dose of sorbent (X_4). The values coded from $-\alpha$ to $+\alpha$ in 1 unit interval, respectively (Table 1). By considering the upper and lower levels of the variables, designing of experiments was performed. Thirty runs for two-level factorial design, 6 replicates for one center point was used to determine the pure errors, and curvature and 8 runs were used for axial points (Table 2) [17]. The runs were divided into blocks; each block contained 20 and 10 runs. The variable interaction was determined by measurement of the response (R) belonged to the adsorption of fluoride by Fe_3O_4@C/La.

2.5. Experimental design studies

The designing of experiments was performed by the Design-expert version 7.0.0 software. The following second-order polynomial model was used to evaluate the independent variables [5]:

$$Y = \beta_0 + \sum_{i=1}^{k} \beta_{ii} x_i^2 + \sum_{i=1}^{k} \beta_{ij} x_i x_i e \quad (1)$$

Prediction of the response Y (removal of F^-) was obtained by the above polynomial. The terms used in the equation are defined as follows: β_0 = intercept term, β_i = linear factor coefficient, x_i and x_j = variable attributed to factors i and j; b_{ii} and b_{ij} = the quadratic factor and the interaction factor coefficients, respectively, k = number of factors, e = the random error.

Data analysis, and dependent and independent variable interaction were studied by variance analysis (ANOVA) [5].

2.6. Adsorption experiments

By performing preliminary experiments, four variables including dosage of adsorbent, solution pH, contact time and F^- content were selected. The experiments were then followed in solution containing 0.1 g of sorbent in 10 mL of fluoride solution (1,000 mg L^{-1}). The mixture was shaken at 25°C for 20 h. The solid was removed and the fluoride content of the solution was determined. According to the Nernst equation, the relationship between the measured potential and F^- concentration was as follows:

$$E = E^0 - 2.303\frac{RT}{F}\log\left[F\right]^- \quad (2)$$

E and E^0 are the potential of the electrode at equilibrium, and the potential of a standard electrode, respectively, R = gas constant, T = temperature (K), F = Faraday constant, and $[F^-]$ = concentration of fluoride. Stock solution

Table 2
Experimental matrix and predicted R for RSM design

Predicted R (mg g^{-1})	Ads. (g) dosage	C F^- (mg L^{-1})	Contact time (min)	pH	Block	Run
1.87	0.1	100.00	260.0	8.00	1	1
18.65	0.05	299.00	260.00	5.00	1	2
20.4	0.05	299.00	90.00	5.00	1	3
12.31	0.05	100.00	90.00	5.00	1	4
8.35	0.05	100.00	260.00	5.00	1	5
6.54	0.08	199.50	175.00	6.50	1	6
2.89	0.1	299.00	90.00	8.00	1	7
3.76	0.1	299.00	260.00	8.00	1	8
8.3	0.1	100.00	260.00	5.00	1	9
13.77	0.05	290.00	260.00	8.00	1	10
2.97	0.1	100.00	90.00	8.00	1	11
8.62	0.1	100.00	90.00	5.00	1	12
7.75	0.08	199.50	175.00	6.50	1	13
4.23	0.1	299.00	90.00	5.00	1	14
19.36	0.05	299.00	90.00	8.00	1	15
7.75	0.08	199.50	175.00	6.50	1	16
6.69	0.05	100.00	90.00	8.00	1	17
7.75	0.08	199.50	175.00	6.50	1	18
7.72	0.1	299.00	260.00	5.00	1	19
4.89	0.05	100.00	260.00	8.00	1	20
25.08	0.03	199.50	175.00	6.50	2	21
10.69	0.08	398.50	175.00	6.50	2	22
18.97	0.08	199.50	175.00	3.50	2	23
0.96	0.08	0.50	175.00	6.50	2	24
8.85	0.08	199.50	175.00	6.50	2	25
7.15	0.08	199.50	5.00	6.50	2	26
7.69	0.08	199.50	345.00	6.50	2	27
8.51	0.13	199.50	175.00	6.50	2	28
9.12	0.08	199.50	175.00	9.50	2	29
8.85	0.08	199.50	175.00	6.50	2	30

SD = 1.04, mean = 9.35, R^2 = 0.9845, adjusted R^2 = 0.9691, predicted R^2 = 0.9041, adequate precision = 31.277 and CV% = 11.13.

Table 1
Coded and actual levels of experimental variables

$+\alpha$	$-\alpha$	Low level (–1)	Mean (0)	High level (+1)	Effective variables	Symbol
9.50	3.50	5	6.50	8	pH	A ($X1$)
345	5	90	175	260	Contact time	B ($X2$)
398.5	0.50	100	199.50	299	C F^-	C ($X3$)
0.125	0.025	0.05	0.075	0.1	Adsorbent dosage	D ($X4$)

(1,000 mg L^{-1}) was prepared by dissolution of 0.221 g of analytical grade NaF in deionized water in a 100 mL volumetric flask, and the calibration curves were constructed in the concentration range of 0.05–1,000 mg L^{-1} [19]. To have a constant ionic strength, 10.0 mL of a solution containing 57.0 mL of CH_3COOH, 58.0 g of sodium chloride and 0.3 g of $Na_3C_6H_5O_7{\cdot}2H_2O$ in 1,000 mL of deionized water known as "total ionic strength adjustment buffer solution" was added to each solution. The flask was then put on a water bath and the pH was adjusted to 5–5.5 by diluted NaOH solution added dropwise into the vessel. The solution was cooled and diluted to volume by deionized water [20].

The fluoride concentration of standard solutions was determined by the fluorine ion electrode and the calibration curve was plotted based on the log [F^-] versus the concentration of standard solutions. The calibration curve was then used to determine the fluoride concentration of samples by the following equation:

$$E = m\log\left[F^-\right] + b \tag{3}$$

E = equilibrium electrode potential, m = slope of the calibration curve, and [F^-] = fluoride content of the solution. The adsorption capacity Q_e (mg g^{-1}) was determined by the following equation:

$$Q = \left(C_0 - C_e\right)\frac{V}{m} \tag{4}$$

C_0 and C_e (mg L^{-1}) = fluoride concentrations before and after adsorption process respectively. V = volume (mL) of the solution, m = weight of sorbent (g) [6].

3. Discussion of the results

3.1. Identification of sorbents

3.1.1. X-ray diffraction patterns

In Fe_3O_4 pattern (Fig. 1a) the diffraction lines appeared at 2θ > 30° (30.1, 35, 42, 54, 62) belonged to the magnetite structure as given in standard pattern (JCPDS file No.19-0629) [12,13].

In the Fe_3O_4@C pattern (Fig. 1b), similar lines were observed at 32, 35.5, 43, 53 and 62.5 showing that the magnetite structure was unchanged during the carbonization process [12,21]. The new broad diffraction bands observed around 2θ = 20 represented the amorphous structure of carbon [13]. In the X-ray diffraction pattern of Fe_3O_4@C/La (Fig. 1c), besides the diffraction lines belonged to Fe_3O_4@C, a new line related to the La_2O_3 structure was appeared at 2θ = 57 indicating that La was immobilized on the surface of the adsorbent. However, owing to the very low content of La (0.49 W%), the peak intensity was very low [15].

3.1.2. FTIR analysis

The FTIR of the samples is given in Fig. 2. For comparison, the FTIR spectrum of reference Fe_3O_4 is shown in Fig. 2a and it is characteristic Fe–O stretching vibration was observed at 576 cm^{-1} [18].

In the FTIR of synthesized Fe_3O_4@C (Fig. 2b), the following absorption bands originated from the appropriate functional groups was observed:

- The wide absorption band at 3,358 cm^{-1} belonged to the stretching vibrations of hydroxide groups [22].
- The peak at 2,923 cm^{-1} region was related to C–H stretching vibrations [22].
- The band at 1,831 cm^{-1} was attributed to the tensile vibrations of –COOH group.
- Absorption band at 1,641 cm^{-1} was attributed to the C=C vibrations, indicating the presence of carbon in the sample [18].
- The band at 1,034 cm^{-1} belonged to O–H bending vibrations, and C–OH stretching [18].
- The presence of the absorption peak at 573 cm^{-1} was related to Fe–O bond vibration of Fe_3O_4 [18].

The FTIR spectrum of Fe_3O_4@C/La adsorbent represented in Fig. 2c comprised of the following absorption bands:

- The absorption peak at 3,355 cm^{-1} belonged to the stretching vibrations of hydroxide groups [22].

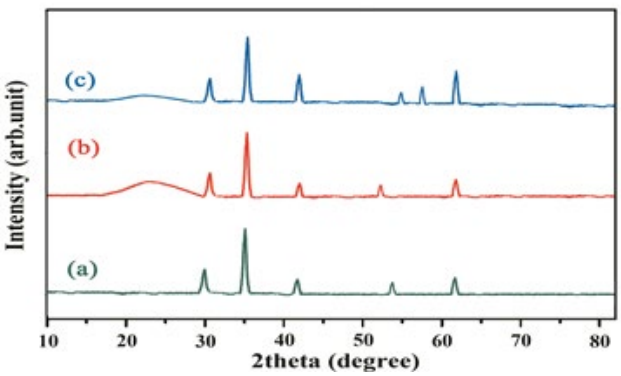

Fig. 1. XRD patterns of Fe_3O_4 (a), Fe_3O_4@C (b), and Fe_3O_4@C/La (c) samples.

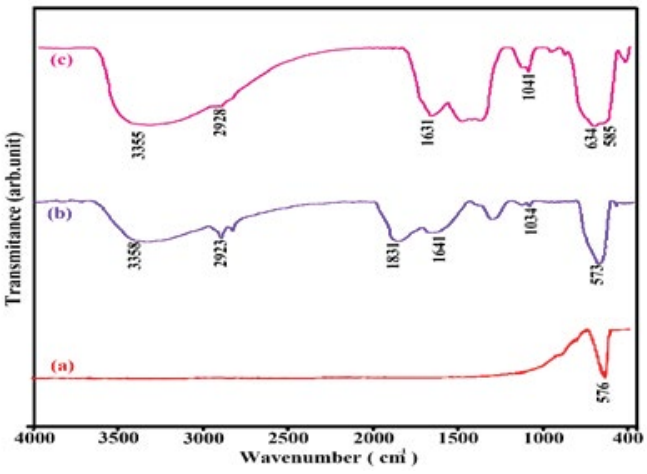

Fig. 2. FTIR spectra of Fe_3O_4 (a), Fe_3O_4@C (b) and Fe_3O_4@C/La (c) samples.

- The weak band at 2,928 cm^{-1} was attributed to the C–H stretching vibrations [22].
- The absorption band at 1,631 cm^{-1} corresponded to the C=C vibrations, and indicated the presence of carbon in the sample [18].
- The peak at 1,041 cm^{-1} resulted from O–H bending vibrations, and C–OH stretching [18].
- The band at 634 cm^{-1} was related to Fe–O bond vibration [18].
- The band at 585 cm^{-1} belonged to La-O absorption band [23].

3.1.3. TEM, SEM images, EDX analysis and map of elements

The TEM image of the Fe_3O_4@C sample represented in Fig. 3a (Mag. 12kx) consisted of mostly spherical particles. Owing to the magnetic interference, the resolution of the image was not very good. However, by a more accurate study of the image, it was revealed that the particle has a magnetite core structure that was surrounded by a less dense carbon layer [18,22]. The core appeared as more black mass indicated the presence of iron oxide crystals and the shells containing carbon particles in the form of opaque, gray and nonuniform eclipses.

From the SEM images of Fe_3O_4@C (Fig. 3b) and Fe_3O_4@C/La (Fig. 3c), it was concluded that both samples had identical morphology. The spherical nanoparticles consisted of Fe_3O_4 as the core and carbon coatings as the shell of the particles. The slight difference in the morphology was attributed to the presence of La on the surface of the Fe_3O_4@C/La sample.

The constituent elements of the composite were identified by EDX analysis (Fig. 1S). In the spectrum, the presence of constituent elements including iron, oxygen, carbon, and lanthanum was observed. The peaks related to iron was originated from magnetic Fe_3O_4, and that belonged to amorphous carbon produced by carbonization of glucose [24]. The map of elements relevant to Fe_3O_4@C/La contains O, Fe, C and La as shown in Fig. 2S. It was concluded that iron and carbon were homogeneously distributed on the structure of composite (Fe_3O_4@C/La).

3.1.4. Porosity of the samples

The BET specific surface areas of Fe_3O_4@C/La were determined by the construction of absorption-desorption nitrogen isotherm (Fig. 4a) [21]. By using Barrett–Joyner–Halenda theory, the void volume, and pore size diameter, and pore distribution were determined (Fig. 4a, inset show). The shape of isotherm was similar to IV-type isotherm according to the classification of the International Union of Pure and Applied Chemistry (IUPAC) [21]. This implied that the pore diameters and the cavities of the sample

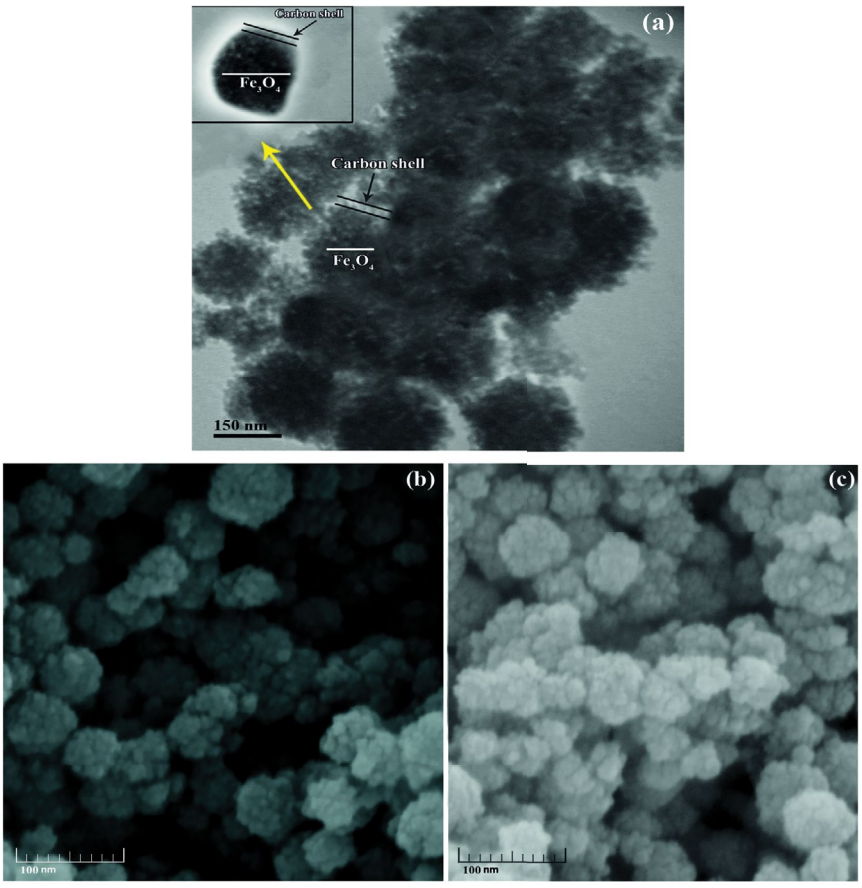

Fig. 3. (a) TEM image of Fe_3O_4@C sample, (b) SEM images of Fe_3O_4@C, and (c) Fe_3O_4@C/La samples.

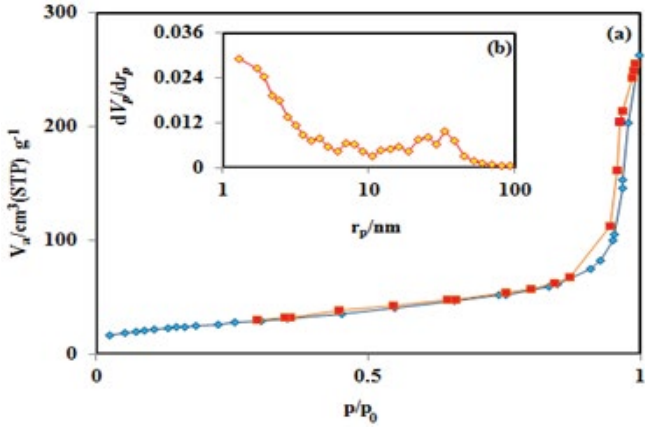

Fig. 4. Nitrogen adsorption–desorption isotherms of Fe_3O_4@C/La (a). Inset shows the Barrett–Joyner–Halenda pore size distribution.

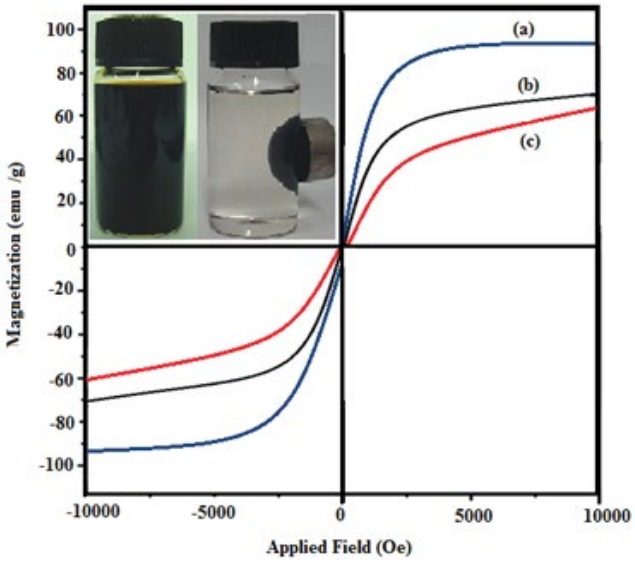

Fig. 5. Saturation magnetization curve of Fe_3O_4 particles (a), Fe_3O_4@C (b), and Fe_3O_4@C/La(c) samples.

were uniform. The specific surface area of Fe_3O_4@C/La was depended on the synthesis method of the Fe_3O_4@C sample because the amount of La deposited on the surface of core-shell was very low. However, the specific surface area and pore volume for Fe_3O_4@C/La in this work were 92.88 $m^2\ g^{-1}$ and 21.336 $cm^3\ g^{-1}$ respectively. The averages pore diameter of Fe_3O_4@C/La was 2.58 nm (Table 3). Based on the IUPAC classification, the Fe_3O_4@C/La sample is classified into the mesopores group of material.

3.1.5. Magnetic property of the adsorbent

The magnetic property of the samples was determined by the VSM technique (Fig. 5). As indicated from the figure, the saturation magnetization of Fe_3O_4 (a), Fe_3O_4@C (b), and Fe_3O_4@C/La (c) 92.80, 70.10, and 60 emu g^{-1} was obtained respectively. The reduction in the magnetization value of Fe_3O_4@C/La was attributed to the formation of the non-magnetic layer on the Fe_3O_4 surface, and the presence of lanthanum on the surface of the magnetic support. However, the magnetization Fe_3O_4@C/La was sufficient for magnetic removal of the sample from aqueous. The sample dispersed in the aqueous medium was readily removed by a magnet bar (Fig. 5, inset show). Reduction on the magnetization after immobilization of a non-magnetic compound on the surface of the magnetic core-shell has already been reported. Kong et al. [13] reported that after the deposition of Pd on the surface of Fe_3O_4@C, its saturation magnetization dropped from 76.8 to 9.7 emu g^{-1}. Zhang and Kong [24] found that the saturated magnetization of Fe_3O_4 was reduced from 92.8 to 38 emu/g^{-1} after the surface of the Fe_3O_4 was covered by carbon. A similar observation was reported by Zhao when they prepared a core-shell structure by grafting of $Al(OH)_3$ on the surface of Fe_3O_4 [25,26].

Table 3
BET characteristics of Fe_3O_4@C/La

Adsorbent	S_{BET} ($m^2\ g^{-1}$)	V_P ($cm^3\ g^{-1}$)	d_P (nm)
Fe_3O_4@C/La	92.88	21.336	2.58

3.2. Experiment design and analysis of data

In the ANOVA section, a quadratic polynomial equation was reported as an empirical model coded for the response variables. The fitness of polynomial was evaluated by the determination of R^2 value. The statistical property was examined by *F*-test, and the terms of the model were examined by *p*-value with a 95% confidence level [5].

The value of R^2 for the selected model corresponds to the Fe_3O_4@C/La was 0.9845. The following regression model for F^- removal was obtained:

$$Y = 8.22 - 2.17X_1 - 0.38X_2 + 2.34X_4 - 4.05X_4 - 0.32X_{12} + 0.62X_{13} - 0.15X_{14} + 0.26X_{23} + 1.00X_{24} - 2.69X_{34} + 1.201X_1^2 - 0.45X_2^2 - 0.85X_3^2 + 1.89X_4^2 \quad (5)$$

(In Eq.) 5), the minus sign of X_3 (F^- concentration) represents the synergistic effect of the variables, while pH (X_1), contact time (X_2), and adsorbent dosage (X_4) had an antagonistic effect. As the fluoride content and solution pH increased, lowers uptake of F^- was obtained.

The solution pH is a major variable affecting the uptake of F^- owing to its influence on charge of adsorbent surface, and also the abundance of F^- ions [26] (Point of zero charge ($pH_{(pzc)}$), is the most significant factor employed to indicate the variation of surface charge by the change of pH. When the pH of the solution was lower than $pH_{(pzc)}$, the sorbent surface had an overall positive charge creating an attractive force towards the negatively charged fluoride ions. Above $pH_{(pzc)}$, the F^- uptake trend became reversed because the surface hydroxide groups are deprotonated and the surface charge of the adsorbent became negative creating a repulsion force between fluoride ions and the adsorbent surface [27].

The results of the analysis of variance for model and its *F* and *p*-values for recognition of the significance of the regression coefficients are reported in Table 4. The model with the highest *F*-values, meaningless lack of fit (LOF) and most values R^2, Adj R^2 and Pred. R^2 will be appropriate if the *p*-value is less than 0.05, the prediction of the results by the model with a 5% confidence level is performed. However, the *p*-value less than 0.0001 confirmed that only 0.01% of the results could produce from noise. The *F*-value of model is significant (F_{cal} = 63.63 > F_c = 2.48), and *p*-value is low (0.0001 < 0.05) when LOF is not significant (F_{cal} = 5.12 < F_c = 5.96). The calculated *p*-value 0.0648 was greater than 0.05 confirmed that the selected model was sufficiently logic. LOF value indicates the data variation is a fitted model. When LOF is nonsignificant it means that the model can describe the data [17]. These contents record that the model for designing the fluoride removal could well describe the data. The entire efficiency of the model can be evaluated from the R^2 value. In this research, the R^2 value for the response of Fe_3O_4@C/La was 0.9845 which showed that the applied model could not explain about 2% of the total variations. The R^2 value also confirmed a relatively good agreement between experimental and predicted results. The estimated R^2 value must be in good agreement with the adjusted R^2 value [17]. If the estimated R^2 value and the adjusted R^2 value are significantly different, it means the insignificant efficiency of the model. The predicted R^2 value indicates the merit of the model for new responses, therefore the R^2 value, and the predicted R^2 must be close [17]. However, the results indicated that the predicted R^2 value (0.9041) was in good agreement with the adjusted R^2 value (0.9691) confirming that no additional variables affected the removal process.

The ratio of predicted responses to their standard deviation is called adequate precision. (AP = 31.277) which, for an acceptable model, this value should be more than 4. In this work, the ratio of 6.27 was obtained which implied that the model was acceptable [17]. The low coefficient of variation (CV% = 11.13) which was obtained in this work validated the obtained data by the model.

Fig. 3S showed that the distribution of data for fluoride uptake was normal [5,28]. The adequacy of the model was also evaluated by plotting the residuals versus predicted values (Fig. 4S). The residuals were randomly scattered around the centerline indicating that no trend was observed on the data [5,17]. From Fig. 6 which shows the plot of internally

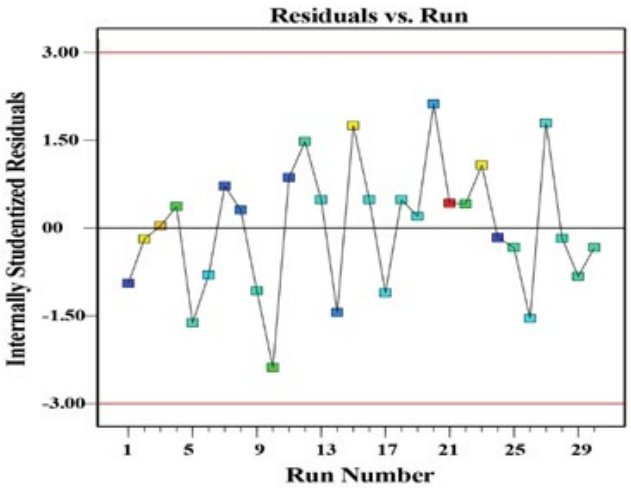

Fig. 6. Residuals vs. run for fluoride removal.

Table 4
ANOVA results of the quadratic model for fluoride removal

Meaningful	*P*-value	*F*-value	Mean squares	d_f	Sum of squares	Source
Significant	<0.00001	63.63	86.83	14	936.62	Model
	<0.00001	104.47	113.01	1	113.01	pH-X_1
	0.0964	3.18	3.44	1	3.44	*t*-X_2
	<0.00001	121.83	131.79	1	131.79	*c*-X_3
	<0.00001	363.92	393.66	1	393.66	*D*-X_4
	0.2422	1.49	1.61	1	1.61	X_1X_2
	0.0315	5.71	6.18	1	6.18	X_1X_3
	0.5763	0.33	0.35	1	0.35	X_1X_4
	0.3298	1.02	1.10	1	1.10	X_2X_3
	0.0017	14.87	16.08	1	16.08	X_2X_4
	<0.00001	107.33	116.10	1	116.10	X_3X_4
	<0.00001	36.74	39.74	1	39.74	$(X_1)^2$
	0.0389	5.19	5.62	1	5.62	$(X_2)^2$
	0.0008	18.37	19.88	1	19.88	$(X_3)^2$
	<0.00001	90.69	98.11	1	98.11	$(X_4)^2$
	–	–	1.08	14	15.14	Residual
Not significant	0.0648	5.12	1.40	10	14.05	Lack of fit
			0.27	4	1.10	Pure error
				29	1,001.79	Total

studentized residuals against the run number of the particular trend was observed indicating that the residuals were independent of runs and were within a particular limit. Therefore, it was assumed that the proposed model was significant and adequate to describe the fluoride uptake by Fe_3O_4@C/La [5,29].

To represent the concurrent influence of duplex parameters on the responses, three-dimensional response surfaces that helps to evaluate the interactions between influencing variables were employed [29]. This was performed by a graphical representation of the results obtained by equation (5). By the plots, the optimum level of each factor was determined, and valuable data regarding the interactions of two independent factors, while the other factors were constant at the corresponding levels were obtained. Accordingly, 3D plots in the removal of F^- by Fe_3O_4@C/La are shown in Fig. 7.

3.3. Interaction of different variables

The interactions of solution pH and contact time are represented in (Fig. 7a). As indicated in the figure the pH is the most influencing variable on the response, because it significantly affects the following reaction (7). Due to the hydrolysis of $La(NO_3)_3$, the produced lanthanum ion is coupled with hydroxide ion (OH^-) existed on the Fe_3O_4@C surface leading to the formation of Fe_3O_4@C-O-La $(OH)_3$ complex and elimination of H^+ [Eq. (6)] [15].

$$Fe_3O_4@C-OH+La(OH)_3 \xrightarrow{-xH^+} \left[Fe_3O_4@C-O-La(OH)_3\right] \quad (6)$$

When a solution containing fluoride ion is adjacent to this complex, the hydroxide ions (OH^-) are displaced with fluoride ions through the ion exchange mechanism (Eq. (7)).

$$\left[Fe_3O_4@C-OLa(OH)_3\right]+xF^- \rightarrow \left[Fe_3O_4@C-O-La(OH)_{3-x}F_x\right]+xOH^- \quad (7)$$

Since the complex consisted of OH^- functional group, the change of the pH affected the uptake of F^- [15]. At higher pHs, the competition between OH^- and F^- leading to lower uptake of the fluoride. At low pH, F^- is converted to HF and its uptake is reduced. Moreover, at very low pH, the lanthanum will partially dissolve in the solution and the adsorption capacity is reduced [16,30]. As indicated in the figure, the maximal uptake of F^- occurred at pH = 5.

To discuss the influence of pH more clearly, pH_{pzc} of the adsorbent was measured (Fig. 5S). It was equal to 5.5 indicating that the adsorbent surface was positively charged at pHs lower than 5.5, and beyond pH = 5.5, the surface charge was positive. The experimental data showed that the maximal adsorption of fluoride was at pH = 5 where the surface was positive and an attraction force was created between the adsorbent surface and fluoride ions.

On the other hand, the figure showed that the process of replacement of fluoride with hydroxide of the complex (Fe_3O_4@C-O-La $(OH)_3$ increased as the contact time increased. Therefore the adsorption of fluoride increased until the equilibrium was established and thereafter the uptake remained constant.

Fig. 7b shows the interaction between the pH and absorbent dose. It was indicated that both variables had a significant influence on the F^- uptake. But the effect of the adsorbent dose was more pronounced than the effect of pH.

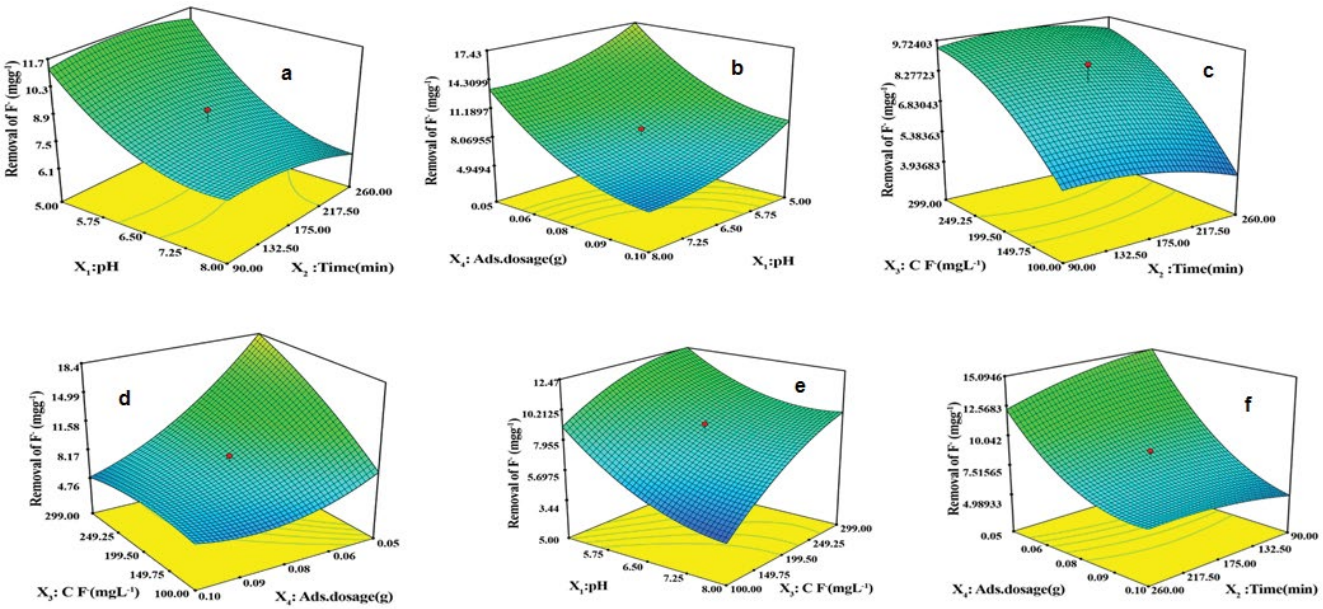

Fig. 7. Response surface plot for fluoride removal as function of (a) pH and contact time, (b) adsorbent dose and pH, (c) fluoride concentration and contact time, (d) fluoride concentration and adsorbent dose,(e) fluoride concentration and pH, and (f) adsorbent dose and contact time.

In fact, with increasing adsorbent dose the uptake of fluoride was lowered. It was assumed that since the measured response was according to mg of fluoride per each gram of adsorbent, by increasing the adsorbent dose each unit mass of the sorbent had a lower impact by the fluoride ions [31].

In Fig. 7c the influence of contacting time and F^- concentration is represented. It was evident that the initial concentration of fluoride had a huge impact on the removal efficiency. By increasing concentration, the number of effective collisions between active sites was increased. However, after optimized value, owing to the saturation of the exchange by increasing the concentration the removal efficiency remained almost at a constant level [27]. The sharp rise in F^- uptake indicated that the sorption of F^- forwarded by diffusion of the ions into the pores of the sorbent [32]. The contact time is an important parameter for fluoride adsorption. The adsorption process initially occurred fast because of the availability of numerous active sites on the adsorbent surface and after 90 min achieved to the equilibrium. After equilibration change on the absorbed F^- was insignificant because of lower accessibility of the active sites and weaker driving force for the adsorption of fluoride [27]. The interaction between other variables including fluoride concentration-pH, contact time- absorbent dose, and concentration-adsorbent dose can be appropriately discussed.

3.4. Process optimization

In this work, the optimal efficiency was obtained at pH = 5, adsorbent dosage = 0.05 g, contact time = 90 min, and F^- conc. = 300 mg L^{-1}, and an experimental run with the desirability of 0.84 among the suggested runs were selected. The experiments were repeated three times. The results indicated that the response (20.75 ± 2.1 (was within 95% confidence interval predicted by the model (22.95 – 19.67) (Table 5) and the results were in agreement with the predicted values.

3.5. Influence of interfering anions

Some anions including SO_4^{2-}, PO_4^{3-}, Cl^-, NO_3^-, CO_3^{2-} and HCO_3^-, are frequently associated with surface and underground water polluted with fluoride ions. These anions may reduce the capacity of adsorbent by engaging of the adsorption sites and lowering the removal of fluoride, particularly when their concentrations are high [5,16,27,30]. In this research, the selectivity of the adsorbent towards fluoride ions was evaluated in the presence of co-existing ions at optimized (conditions (pH = 5, adsorbent dose = 0.05 g, fluoride concentration = 300 mg L^{-1} and contacting time time = 90 min). Briefly, a series of solution containing 50, 100, 200, and 400 mg L^{-1} of each anion was prepared, the optimized conditions for fluoride removal was adjusted, and the uptake of fluoride was measured. The influence of anions on the uptake of F^- is shown in Table 6. Limit of disturbance is defined as the concentration of anion which causes an error greater than ±5% on the fluoride adsorption. The results showed that F^- uptake in a solution containing 200 mg L^{-1} of interfering anions was reduced to 95.32% and 95.06%, respectively for Cl^- and NO_3^- and with a concentration of 100 mg L^{-1}, 95.75% and 95.2% for, HCO_3^-, OH^- respectively. Therefore, the effect of HCO_3^- and OH^- was more pronounced than that of Cl^- and NO_3^- because the presence of HCO_3^- and OH^- besides the completion of the anions for the adsorption sites changed the pH of the solution which in turn affected on the removal of fluoride [31]. The charge density of the co-existing anion is also a determinant parameter on their interfering effect [26].

3.6. Regeneration of the adsorbent

The economic adequacy of each sorbent depends on its regeneration performance. In this work, the regeneration of sorbent in acidic media pH was imperfect, while in alkaline pH the loaded F^- was leached out [26].

Therefore, the regeneration was performed by the use of NaOH solution (2 M) [15]. After adding 25 ml of NaOH solution to 0.05 g of the used sorbent, the mixture was agitated for 5 h at 25°C. The sorbent was removed and the concentration of the released fluoride was measured. The adsorbent was thoroughly washed with deionized water and then subjected to the removal of fluoride under optimized conditions. The adsorption/ regeneration process was repeated three times (Fig. 8). It was concluded that the NaOH solution was a good eluent for the regeneration of Fe_3O_4@C/La, and about 73% of the adsorbent capacity remained after the third regeneration step.

4. Conclusions

In summary, Fe_3O_4@C core-shell nanoparticles were successfully synthesized by the solvothermal method and Fe_3O_4 nanoparticles were readily encapsulated on a carbon shell. Lanthanum modified magnetic core-shell (Fe_3O_4@C/La) showed good adsorption performance for fluoride uptake from aqueous solutions. The optimal conditions for fluoride

Table 5
Results of experimental runs compared with the predicted values by the model

Variable	pH	Contact time	C F^-	Adsorbent dosage
Optimized values	5	90	299	0.05
Suggested model	Quadratic			
Predicted response	21.30			
95% Cl low and high	19.67–22.95			
Predicted standard deviation	3.70			
Observed response (n = 3)	20.75 ± 2.1			

Table 6
Effect of co-existing anions on fluoride sorption

Interfering ion	Ion concentration (mg L^{-1})	Removal%	–Error%
Cl^-	0	100	–
	50	97.79	2.21
	100	97.27	2.73
	200	95.32	4.68
	400	94.65	5.35
NO_3^-	0	100	–
	50	97.67	2.33
	100	96.67	3.33
	200	95.06	4.94
	400	94.40	5.60
HCO_3^-	0	100	–
	50	97.40	2.60
	100	95.75	4.25
	200	94.31	5.69
	400	91.06	8.94
OH^-	0	100	–
	50	96.38	3.62
	100	95.20	4.80
	200	90.89	9.11
	400	78.44	21.56

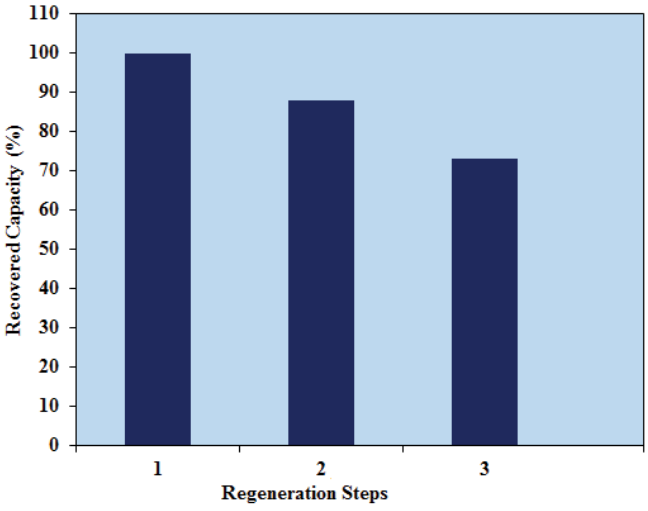

Fig. 8. Regeneration of Fe_3O_4@C/La adsorbent.

adsorption were obtained via the surface response method. The influence of each variable on the adsorption process was determined by the quadratic polynomial equation proposed by the software. By using the ANOVA, and according to the R squares (R^2 = 0.9845) and adjusted R squares (Adj R^2 = 0.9691), the model agreed with the results. Among different studied variables, pH had the most influence and time had the least impact on the adsorption of fluoride. At optimized conditions, the adsorption capacity of 20.75 mg g^{-1} was obtained. The results indicated that the presence of Cl^- had no significant effect on the uptake of F^-, while OH^- significantly reduced the fluoride uptake. The results of reusability tests demonstrated that the Fe_3O_4@C/La was regenerated by washing with NaOH solution.

References

[1] K.E. Wiemer, A. Anderson, B. Stewart, The importance of water quality for media preparation, Hum. Reprod., 13 (1998) 166–172.
[2] H.N. Sahoo, M. Mahapatra, G. Sabat, L. Patra, R. Padhy, B.K. Mohanty, Analysis of potable water quality in berhampur town Odisha, Int. J. Plant Anim. Environ. Sci., 6 (2016) 72–76.
[3] D. Thakre, P. Dixit, S. Waghmare, N. Manwar, N. Labhsetwar, S.S. Rayalu, Synthesis optimization and fluoride uptake properties of high capacity composite adsorbent for defluoridation of drinking water, Environ. Prog. Sustainable Energy, 34 (2015) 1576–1585.
[4] V. Tomar, D. Kumar, A critical study on efficiency of different materials for fluoride removal from aqueous media, Chem. Cent. J., 7 (2013) 2–15.
[5] M.R. Samarghandi, M. Khiadani, M. Foroughi, H. Zolghadr Nasab, Defluoridation of water using activated alumina in presence of natural organic matter via response surface methodology, Environ. Sci. Pollut. Res. Int., 23 (2017) 887–897.
[6] S.S. Waghmare, T. Arfin, N. Manwar, D. Lataye, N. Labhsetwar, S. Rayalu, Preparation and characterization of *Polyalthia longifolia* based adsorbent for removing fluoride from drinking water, Asian J. Adv. Basic Sci., 4 (2015) 12–24.
[7] C.P. Bergmann, F. Machado, Carbon Nanomaterials as Adsorbents for Environmental and Biological Applications, Springer, Berlin, 2015.
[8] P. Sharma, K. Sen, P. Thakur, M. Chauhan, K. Chauhan, Spherically shaped pectin-g-poly(amidoxime)-Fe complex: a promising innovative pathway to tailor a new material in high amidoxime functionalization for fluoride adsorption, Int. J. Biol. Macromol., 140 (2019) 78–90.
[9] J.J. Garcia-Sancheza, M. Solache-Riosb, J.M. Martinez-Gutierrezc, N.V. Arteaga-Lariosc, M.C. Ojeda-Escamillac, I. Rodriguez-Torresa, Modified natural magnetite with Al and La ions for the adsorption of fluoride ions from aqueous solutions, J. Fluorine Chem., 186 (2016) 115–124.
[10] M. Bhaumik, T.Y. Leswifi, A. Maity, V.V. Srinivasu, M.S. Onyango, Removal of fluoride from aqueous solution by polypyrrole/Fe_3O_4 magnetic nanocomposite, J. Hazard. Mater., 186 (2011) 150–159.
[11] C. Zhang, L. Chen, T.J. Wang, C.L. Su, Y. Jin, Synthesis and properties of a magnetic core–shell composite nano-adsorbent for fluoride removal from drinking water, Appl. Therm. Eng., 317 (2014) 552–559.
[12] Y. Du, W. Liu, R. Qiang, Y. Wang, X. Han, J. Ma, P. Xu, Shell thickness-dependent microwave absorption of core–shell Fe_3O_4@C composites, ACS Appl. Mater. Interfaces, 6 (2014) 12997–13006.
[13] L. Kong, X. Lu, X. Bian, W. Zhang, C. Wang, Constructing carbon-coated Fe_3O_4 microspheres as antiacid and magnetic support for palladium nanoparticles for catalytic applications, ACS Appl. Mater. Interfaces, 3 (2011) 35–42.
[14] K. Aguilar-Arteaga, J.A. Rodriguez, E. Barrado, Magnetic solids in analytical chemistry: a review, Anal. Chim. Acta, 674 (2010) 157–165.
[15] E. Vences-Alvarez, L.H. Velazquez-Jimenez, L.F. Chazaro-Ruiz, P.E. Diaz-Flores, J.R. Rangel-Mendez, Fluoride removal in water by a hybrid adsorbent lanthanum-carbon, J. Colloid Interface Sci., 455 (2015) 194–202.
[16] Y. Yu, C. Wang, X. Guo, J.P. Chen, Modification of carbon derived from *Sargassum* sp. by lanthanum for enhanced adsorption of fluoride, J. Colloid Interface Sci., 441 (2015) 113–120.
[17] H. Dericvandi, A. Nezamzadeh-Ejhieh, Designing of experiments for evaluating the interactions of influencing factors on the photocatalytic activity of NiS and SnS_2: focus on coupling, supporting and nanoparticles, J. Colloid Interface Sci., 490 (2017) 628–641.

[18] J. Zheng, Z.Q. Liu, X.S. Zhao, M. Liu, X. Liu, W. Chu, One-step solvothermal synthesis of Fe_3O_4@C core-shell nanoparticles with tunable sizes, Nanotechnology, 23 (2012) 165–601.
[19] Z. Luo, M. Guo, H. Chen, Z. Lian, W. Wei, Determining fluoride ions in ammonium desulfurization slurry using an ion selective electrode method, IOP Conf. Ser.: Earth Environ. Sci, 121 (2018) 1–6.
[20] M. Ansari, M. Kazemipour, M. Dehghani, M. Kazemipour, The defluoridation of drinking water using multi-walled carbon nanotubes, J. Fluorine Chem., 132 (2011) 516–520.
[21] S. Sang, H. Zhang, Y. Sun, A. Jian, W. Zhang, Facile synthesis of carbon-encapsulated Fe_3O_4 core/shell nanospheres for application in Pb(II) electrochemical determination, Int. J. Electrochem. Sci., 12 (2017) 1306–1317.
[22] R. Wu, J.H. Liu, L. Zhao, X. Zhang, J. Xie, B. Yu, X. Ma, S.T. Yang, H. Wang, Y. Liu, Hydrothermal preparation of magnetic Fe_3O_4@C nanoparticles for dye adsorption, J. Environ. Chem. Eng., 2 (2014) 907–913.
[23] H. Saravani, M. KhaJehali, Synthesis and characterization of lanthanum oxide and lanthanum oxide carbonate nanoparticles from thermalizes of [La(acacen)(NO_3)(H_2O) complex, Orient. J. Chem., 32 (2016) 491–498.
[24] Z. Zhang, J. Kong, Novel magnetic Fe_3O_4@C nanoparticles as adsorbents for removal of organic dyes from aqueous solution, J. Hazard. Mater., 193 (2011) 325–329.
[25] X. Zhang, M. He, J.H. Liu, R. Liao, L. Zhao, J. Xie, R. Wang, S.T. Yang, H. Wang, Y. Liu, Fe_3O_4@C nanoparticles as high-performance Fenton-like catalyst for dye decoloration, Chin. Sci. Bull., 59 (2014) 3406–3412.
[26] X. Zhao, J. Wang, F. Wu, T. Wang, Y. Cai, Y. Shi, G. Jiang, Removal of fluoride from aqueous media by Fe_3O_4@$Al(OH)_3$ magnetic nanoparticles, J. Hazard. Mater., 173 (2010) 102–109.
[27] A. Dhillon, M. Nair, S.K. Bhargava, D. Kumar, Excellent fluoride decontamination and antibacterial efficacy of Fe-Ca-Zr hybrid metal oxide nanomaterial, J. Colloid Interface Sci., 1 (2015) 289–297.
[28] H. Derikvandi, A. Nezamzadeh-Ejhieh, Comprehensive study on enhanced photocatalytic activity of heterojunction ZnS-NiS/zeolite nanoparticles: experimental design based on response surface methodology (RSM), impedance spectroscopy and GC-MASS studies, J. Colloid Interface Sci., 490 (2017) 652–664.
[29] M. Nosuhi, Al. Nezamzadeh-Ejhieh, High catalytic activity of Fe(II)-clinoptilolite nanoparticales for indirect voltammetric determination of dichromate: Experimental design by response surface methodology (RSM), Electrochim. Acta., 223 (2017) 47–62.
[30] Z. Yi, X. Ying, C. Hao, L. Bingjie, G. Xiang, W. Dongfen, L. Peng, La(III)-loaded bentonite/chitosan beads for defluoridation from aqueous solution, J. Rare Earths, 32 (2014) 458–466.
[31] S.P. Kamble, S. Jagtap, N.K. Labhsetwar, D. Thakare, S. Godfrey, S. Devotta, S.S. Rayalu, S.P. Kamble, S. Jagtap, N.K. Labhsetwar, Defluoridation of drinking water using chitin, chitosan and lanthanum-modified chitosan, Chem. Eng. J., 129 (2007) 173–180.
[32] S.S. Tripathy, J.L. Bersillon, K. Gopal, Removal of fluoride from drinking water by adsorption onto alum-impregnated activated alumina, Sep. Purif. Technol., 50 (2006) 310–317.

Supplementary information

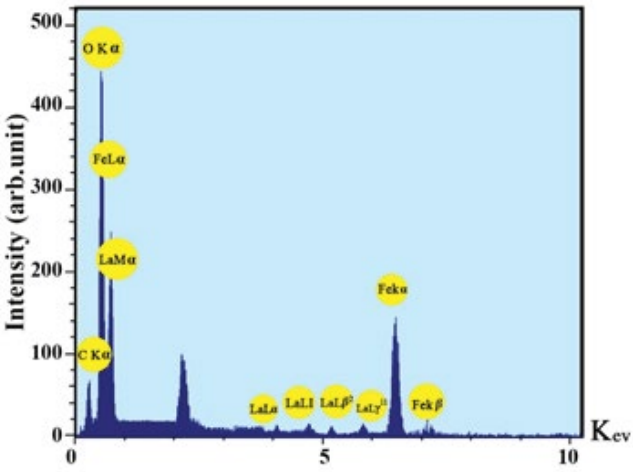

Fig. 1S. EDX spectrum of Fe_3O_4@C/La.

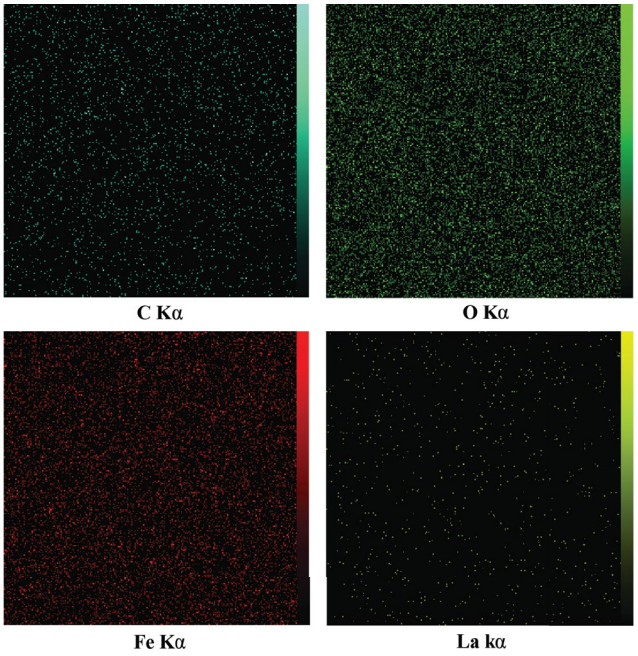

Fig. 2S. X-ray map of Fe_3O_4@C/La.

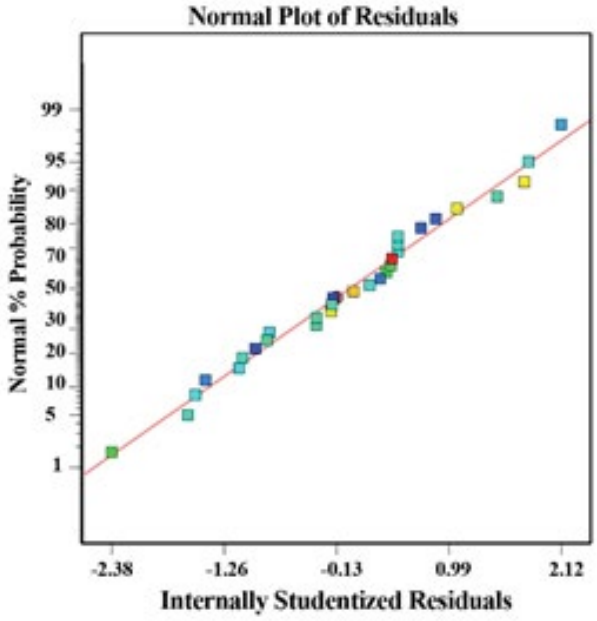

Fig. 3S. Normal probability of residuals of fluoride removal.

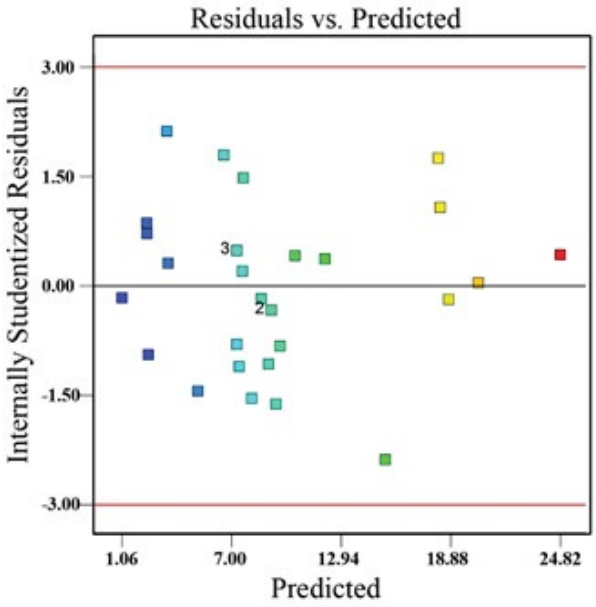

Fig. 4S. Residuals vs. predicted for fluoride removal.

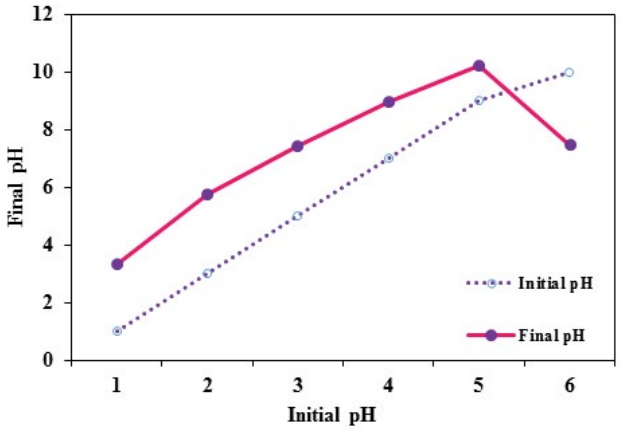

Fig. 5S. Graph of the measurement of pHpzc of Fe_3O_4@C/La and comparison with optimal pH.